Front. Chem. Sci. Eng. 2023, 17(7): 906–917
https://doi.org/10.1007/s11705-022-2273-9

RESEARCH ARTICLE

In situ preparation of Ag@AgCl/Bio-veins composites and their photocatalytic activity and recyclability

Min Zou[1,2*], Chao Tan[3*], Zhengqiu Yuan (✉)[2], Ming Wu[2], Jian Jian[2], Lei Zhang[2], Yan Zhang[2], Zhou Ma[2], Hu Zhou (✉)[2]

1 School of Resource & Environment and Safety Engineering, Hunan University of Science and Technology, Xiangtan 411201, China
2 Key Laboratory of Theoretical Organic Chemistry and Functional Molecules, Ministry of Education, Functional Film Materials Engineering Research Center of Hunan Province, Hunan Provincial Key Laboratory of Advanced Materials for New Energy Storage and Conversion, School of Chemistry and Chemical Engineering, Hunan University of Science and Technology, Xiangtan 411201, China
3 School of Information and Electrical Engineering, Hunan University of Science and Technology, Xiangtan 411201, China

Abstract The industrial application of nano-photocatalysts in wastewater treatment has been severely restricted for a long time due to their difficult separation, poor reusability, and low efficiency. In this work, a facile strategy was proposed to enhance the photocatalytic activity and recovery performance of Ag@AgCl nanocatalysts. Biological veins (Bio-veins) with a unique 3D porous construction were used as carriers for the *in-situ* growth of Ag@AgCl nanoparticles. Scanning electron microscopy results showed that the Ag@AgCl nanoparticles were uniformly loaded on the surface and interior of the Bio-veins, and the size of the Ag@AgCl nanoparticles immobilized on the Bio-veins (50–300 nm) was significantly smaller than Ag@AgCl obtained by the co-precipitation method (1–3 μm). The Bio-veins played a vital role in the photocatalysis reaction system. The degradation efficiency of the Ag@AgCl/Bio-veins(CI4) was up to 3.50 times as high as pure Ag@AgCl. Furthermore, the composites also exhibited excellent recyclability and stability under both visible and solar light. This work provided a suitable strategy for nano-photocatalysts for practical application and may also offer new possibilities for the high-value utilization of biomass materials.

Keywords Ag@AgCl, biological veins, photocatalytic activity, recyclability

Received July 26, 2022; accepted October 16, 2022

E-mails: yuanzhengqiu@126.com (Yuan Z.),
hnustchemzhou@163.com (Zhou H.)

* These authors contributed equally to this work.

1 Introduction

With the rapid development of industry, synthetic dyes as coloring materials have been widely applied in various fields, such as in textile, printing, plastic, leather, cosmetics, and photosensitive materials [1–3]. By 2020, the global annual consumption of synthetic dyes was as high as 7500000 tons [4]. The extensive use of dyes can be considered a double-edged sword, adding beautiful color in our lives while also causing considerable environmental harm. The effective and environmental treatment of dyestuff wastewater with a high concentration, strong toxicity, and refractory organic dyes has been studied in detail. Currently, common methods for treating dye wastewater mainly include coagulation, adsorption, biodegradation, ozonation and photodegradation [5–7]. Among these, photocatalysis has shown to be promising technique due to its environmental friendliness, simple operation, low cost, and lack of secondary pollution generation [8–10].

Nanostructured silver particles (Ag NPs), a type of common noble metal particle, have attracted increasing attention in the photocatalysis field in recent years. These noble metal particles can efficiently absorb visible light via the strong localized surface plasmon resonance (LSPR) effect [11,12]. Furthermore, Ag NPs present distinctive physico-chemical properties such as good antibacterial activity, high electrical conductivity, excellent magnetic performance, and chemical stability. Thus, they have been widely used for disinfection and photodegradation [13,14]. Based on these factors, numerous studies have indicated that nanocomposite photocatalysts combining Ag NPs with other semiconductors, such as clinoptilolite-supported Ag/TiO_2 [15], Ag@AgCl [16],

$Ag@Ag_3PO_4$ [17], and Ag/AgCl/ZnO [18], will always possess stronger photocatalytic activities than pure Ag NP photocatalysts. Specifically, the Ag NPs that formed on silver chloride particles displayed outstanding visible light response and highly enhanced photocatalytic properties due to the LSPR of Ag. Although Ag@AgCl semiconductor photocatalysts will exhibit excellent catalytic performance, most Ag@AgCl semiconductors prepared by conventional methods will be in powder form, and powdery Ag@AgCl photocatalysts still have several shortages that greatly limit their applications [19,20]: (1) Specifically, the high surface energy of powdery nano-photocatalysts will cause them to easily agglomerate and be difficult to disperse in aqueous solutions, thus, greatly decreasing their photocatalytic activity and stability; (2) the separation and recycling of micro-sized or nano-sized powdery catalysts from the solution will be a highly difficult and high-cost process, where the residual catalyst may lead to secondary contamination. Considering these problems, many researchers are trying to find suitable substrates for immobilizing Ag@AgCl NPs.

Biomass materials have attracted the attention of environmental experts due to their innocuity, low cost, and renewability [21]. Many studies have successfully loaded nanocatalysts onto various biomass materials. For example, Gao et al. [22] used corn cob powder as the carbon source to fabricate $C/Fe_3O_4/Bi_2O_3$ and the composite photocatalyst showed a high removal ability for tetracycline. Xu et al. [23] proposed a novel pyrolysis-loading process to load zero-valent irons on biochar, where the obtained BC-ZVI could efficiently adsorb As(III) and As(V). Combining the pyrolysis process with ultrasonication, Alsaiari successfully prepared AC/TiO_2 nanocomposites, and the used biomass AC was processed from date seeds [24]. New TiO_2-carbon microsphere composite materials were synthesized by Peñas-Garzón et al. [25] through the solvothermal procedure, presenting good visible light degradation performance towards diclofenac. However, the biomass materials mentioned above were used in the form of carbon, and the preparation processes required high energy consumption and complex operation. Until now, few researchers have attempted to directly use natural biomass to support nano-photocatalysts. In our previous study [26], we successfully loaded BiOBr nanosheets on the vein surfaces of a natural Osmanthus tree leaf through a simple wet dripping process. The main components of the natural leaf veins were cellulose, hemicellulose and lignin, and these substances were non-toxic and biodegradable. Second, there were abundant hydroxyl (–OH) and carboxyl (–COOH) groups in the long chains in the molecular structures of the leaf veins, providing a benefit to the adsorption of metal-precursor and pollutant molecules [27,28]. Third, the leaf veins with a 3D ramified architecture could provide plenty of space for the growth of the photocatalyst nanoparticles. Moreover, the leaf veins were lightweight and flexible, enabling the vein-based photocatalysts to float on the wastewater, which could greatly simplify the separation and recovery process of the nanocomposites. Using the natural leaf veins as a photocatalyst carrier was verified to be a feasible and promising strategy.

In this study, Ag@AgCl particle hybrid lignocellulosic leaf veins (Ag@AgCl/Bio-veins) were prepared using a simple *in situ* method. Due to the abundant functional groups and unique 3D reticular structure of the biological veins, the Ag@AgCl particles were uniformly distributed and firmly immobilized on the surface and inside of the Bio-veins, realizing the high photoactivity of the hybrid materials. Furthermore, the lignocellulosic Bio-veins could effectively adsorb the dye molecules, which was also advantageous to the photodegradation of RhB. Finally, the Ag@AgCl/Bio-veins(CI4) was composite used to degrade RhB under natural sunlight irradiation, showing satisfactory photodegradation efficiency. This easily prepared, cost-effective Bio-veins based catalyst not only displayed high photodegradation performance but also possessed excellent recyclability and stability.

2 Experimental

2.1 Materials

$AgNO_3$, NaCl, NaOH, isopropyl alcohol (IPA), triethanolamine (TEOA), and 4-hydroxy-TEMPO (TEMPO) were obtained from Shanghai Aladdin Industrial Inc. H_2O_2 (3%–3.5%) was purchased from Henan Liuhe Pharmaceutical Group Co. Ltd. Rhodamine B (RhB) was provided by the Shanghai Kaifei Biomedical Technology Co. Ltd. All reagents used in this work were used directly after purchase and deionized water was employed in the experiments.

2.2 Bio-veins processed from natural leaves

Figure 1 shows the synthesis of the Bio-veins and the Ag@AgCl/Bio-veins. The Bio-veins matrices used for immobilizing the catalyst were processed from natural leaves, which were treated with NaOH and H_2O_2 solution to remove the mesophyll and pigment. The detailed treatment process for the Bio-veins is shown in Fig. 1(a). Leaves from *Osmanthus fragrans* trees were picked on the campus of the Hunan University of Science and Technology. First, the freshly picked leaves were cleaned with deionized water to remove dust. Then, about 20 cleaned leaves were immersed in NaOH aqueous solution (10 wt %, 300 mL) and boiled for 2 h. The softened leaves were transferred to a petri dish with a small amount of deionized water, and a clean toothbrush was used for cleaning to remove the mesophyll, to obtain the

naked leaf veins matrices. After rinsing in deionized water, the wet veins were placed in H_2O_2 solution (3.5 wt %, 200 mL) for 24 h to remove the pigment. Finally, the leaf veins were washed thoroughly and dried for 2 h in a freeze drier. The prepared *Osmanthus fragrans* leaf veins sample was labeled as Bio-veins.

2.3 Synthesis of Ag@AgCl/Bio-veins

The Ag@AgCl/Bio-veins was prepared by impregnation–precipitation and photoreduction methods. Figure 1(b) shows the detailed synthesis process, where first, one piece of Bio-veins with a dry weight of 60 mg was immersed in 30 mL of 0.025 mol·L^{-1} $AgNO_3$ aqueous solution for 30 min, taken out, and immersed in deionized water for 4 s. Then, the Bio-veins was transferred to 30 mL of 0.025 mol·L^{-1} NaCl aqueous solution for 30 min, removed and immersed in deionized water for 4 s. The above operations were carried out in the dark at room temperature and the four soaking steps were defined as a cycle. To determine the optimal cycle time, samples with different cycle times (1, 2, 3, and 4) were synthesized. With an increase in cycle time, yellowish-green Bio-veins became white, indicating that the AgCl NPs successfully grew onto the Bio-veins. After washing with deionized water three times, the AgCl/Bio-veins composites were freeze-dried. Finally, the AgCl/Bio-veins composites were subjected to a 36 W ultraviolet light for 10 min and the color changed to black, from which we could infer that some of the Ag^+ ions were successfully reduced to Ag^0. According to the impregnation cycle times, the prepared samples were denoted as Ag@AgCl/Bio-veins(CI1), Ag@AgCl/Bio-veins(CI2), Ag@AgCl/Bio-veins(CI3), and Ag@AgCl/Bio-veins(CI4).

2.4 Characterization analysis

The phase structure of the as-synthesized materials was detected by powder X-ray diffraction (XRD, Bruker D8-Advance). Scanning electron microscopy (SEM, JSM-7610FPlus, JEOL) was employed to observe the surface and cross-section morphologies of the obtained photocatalysts. A Fourier transform infrared spectrophotometer (FTIR, Thermo Fisher, Nicolet 6700) was employed to characterize the functional groups of the synthesized materials. X-ray photoelectron spectroscopy (XPS, Thermo Scientific K-Alpha) was used to study the surface composition and chemical states of Ag@AgCl/Bio-veins composite in an ultrahigh vacuum electron spectrometer (Al Ka X-ray radiation). The optical property of synthesized materials was tested by a UV–vis diffuse reflectance spectroscopy (DRS, UV–2550, Shimadzu).

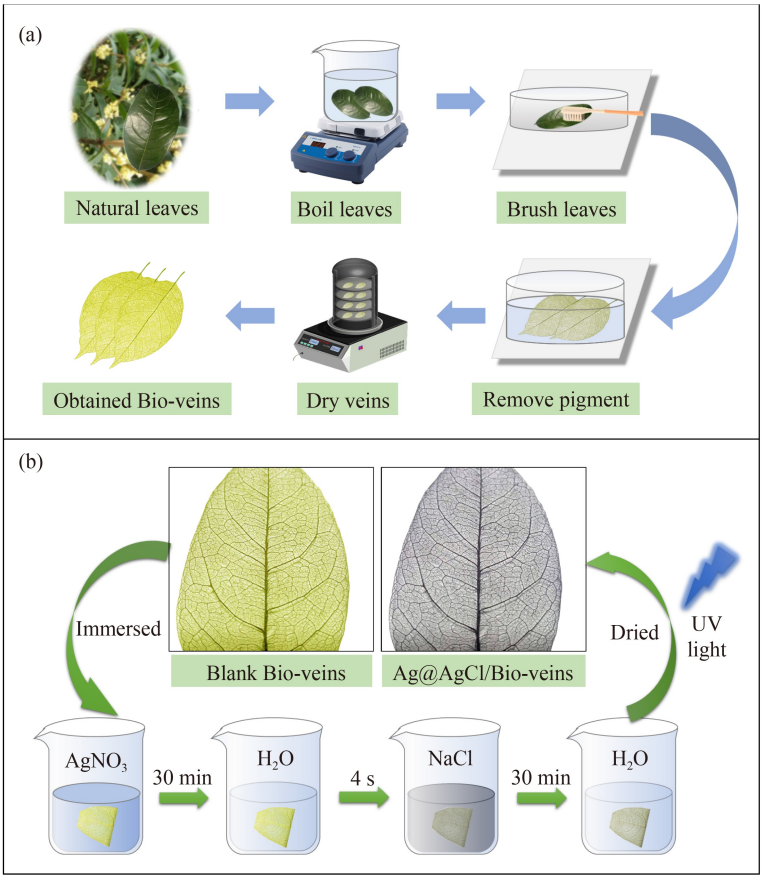

Fig. 1 Schematics showing the synthesis of (a) Bio-veins and (b) Ag@AgCl/Bio-veins.

2.5 Photocatalytic activity test

For the visible photocatalytic experiments, a 300 W xenon lamp with a long pass filter ($\lambda > 420$ nm) was used as the visible light source. A homemade top-irradiation double-layer quartz container was used as the photocatalytic reactor, and 10 mg·L^{-1} RhB solution was employed to simulate the dye effluent. The vertical distance between the bottom of the reactor and lamp was 20 cm, the speed of the magnetic stirrer was maintained at 300 r·min^{-1}, and the temperature of the reaction system was kept at room temperature by using cooling recycled water. In a typical procedure, a piece of Bio-veins loading Ag@AgCl was placed in the reactor with 100 mL of RhB solution. The mixture was stirred in dark conditions for 30 min to achieve adsorption–desorption equilibrium. Then, they were exposed to the xenon lamp, at 10 min intervals, and 5 mL of solution was sampled out by a pipette. After centrifugation (8000 r·min^{-1}, 5 min), about 3 mL of the sample supernatant was suctioned out and was used to measure the residual concentration of RhB via UV–vis absorption spectroscopy (UV-1800PC, Shanghai Aoyi Instrument Co. Ltd).

For the cycling tests, all of the conditions and parameters were consistent with the above experiment. After every photocatalytic reaction, the leaf-shaped Ag@AgCl/Bio-veins photocatalyst was taken out by a tweezer and washed alternately with deionized water and absolute ethanol three times to remove the attached undegraded RhB. After freeze drying for 2 h, the recycled photocatalyst was used directly for the next photocatalytic cycle experiment.

For the solar photocatalytic experiments, a piece of hybrid Ag@AgCl/Bio-veins(CI4) composite was put into a beaker with 100 mL of RhB (10 mg·L^{-1}). Then they were placed in the sun from 9:00 am to 14:00 pm, where the outdoor temperature ranged from 20 to 26 °C. In addition, the intensity of sunlight on the test days were measured and recorded by an optical power meter (PM120D, Thorlabs, America). The lowest value of light intensity was 11.77 mW·cm^{-2} and the maximum value was 20.83 mW·cm^{-2}.

3 Results and discussion

3.1 Characterization of the photocatalysts

3.1.1 Crystalline structure

The XRD patterns of the as-prepared products are shown in Fig. 2, and as shown in Fig. 2(a), the broad peaks in Bio-veins situated at 2θ = 17.0° and 2θ = 23.0° are assigned to cellulose I of cellulose and lignin. For pure AgCl, a series of peaks at 2θ = 28.0°, 32.3°, 46.4°, 55.0°, 57.7°, 67.7° and 76.8° are well indexed to the (111), (200), (220), (311), (222), (400), (331) and (420) faces of the three dimensional face-centered cubic phase of AgCl (JCPDS No. 31-1238) [29]. All of these peaks are also present in the Ag@AgCl/Bio-veins(CI4) composite, demonstrating that the AgCl NPs successfully grow on the Bio-veins matrices and the introduction of Bio-veins does not affect the crystalline structure of AgCl. In addition, a weak peak located at 2θ = 38.5° is also observed, corresponding to the (111) plane of metallic Ag (JCPDS No. 04-0783). This indicates that some of the Ag^+ ions in the AgCl particles are successfully converted into Ag NPs [30]. We also find that the intensities of the peaks at 17.0° and 23.0° decrease with an increase in circulation time (Fig. 2(b)), likely because the Bio-veins surface is covered by a large quantity of Ag@AgCl NPs. The XRD results indicate that the as-fabricated composite photocatalytic materials contain crystalline AgCl as well as Ag.

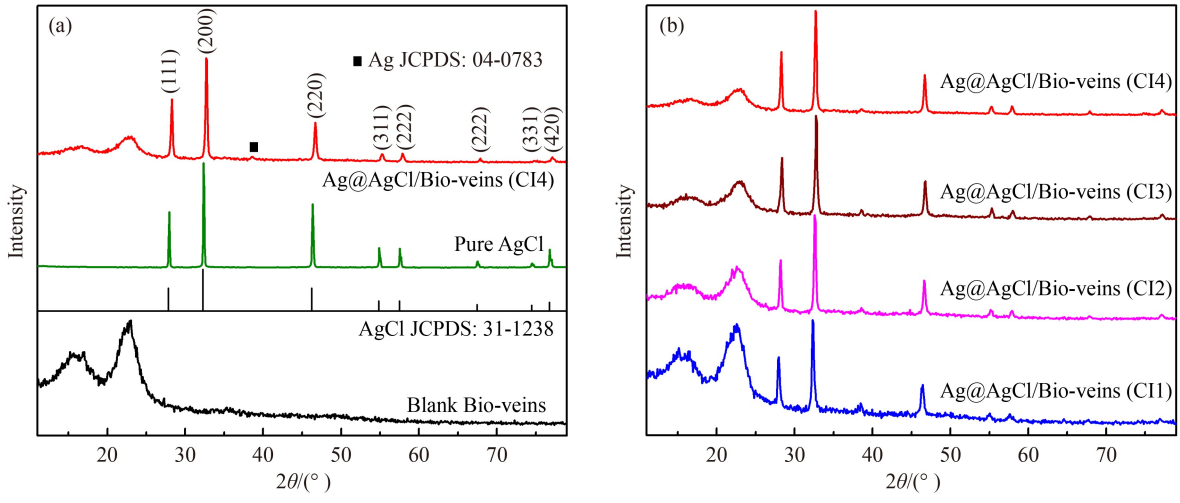

Fig. 2 XRD patterns of (a) Bio-veins, AgCl, Ag@AgCl/Bio-veins(CI4) composite, and (b) Ag@AgCl/Bio-veins(CI1, CI2, CI3, CI4) composites.

3.1.2 Morphology structure

SEM was applied to observe the internal structure of Bio-veins and to investigate the morphologies of the Ag@AgCl NPs. As shown in the first row of Fig. 3, the naked Bio-veins possess a distinctive branching structure, where the surface of the dendritic fiber is flat and smooth. After the *in-situ* synthesis process, cubic-like Ag@AgCl NPs are successfully grown on the fiber face of the Bio-veins (second row in Fig. 3). With increased soaking cycle time, the Ag@AgCl NP loading amount continuously increases, and the Ag@AgCl NPs are spread evenly on the fibers without any agglomeration. Through careful contrast and analysis of the SEM images of the Ag@AgCl/Bio-veins composites with pure Ag@AgCl (Figs. 3(i–k)), we find a significant difference between the sizes and shapes of the Ag@AgCl NPs. The size of the Ag@AgCl NPs fixed on the Bio-veins (50–300 nm) is significantly smaller than pure Ag@AgCl (1–3 μm). The composition of the Ag@AgCl/Bio-veins(CI4) composite was assessed by EDS. As shown in Fig. 3(l), we further confirm that the composite contains C, O, N, Ag, and Cl elements. By comparing the cross-sectional micrographs of the blank Bio-veins and Ag@AgCl/Bio-veins(CI4) composite (Figs. 3(m–p)), we find that the Ag@AgCl nanocomposites also grow on the inner microfibril walls of the Bio-veins, and the microstructures of the Bio-veins are well-maintained. In this study, the Bio-veins as stable carriers play a very important role, and could not only immobilize the Ag@AgCl NPs effectively and prevent their aggregation, but also affect the morphology and structure of the particles. The Ag@AgCl NPs that grow *in situ* on Bio-veins surfaces exhibit a larger surface area and better dispersion, which is favorable for the higher photocatalytic activity of the Ag@AgCl/Bio-veins.

3.1.3 FTIR, DRS, and XPS spectroscopy

The FTIR spectra of the blank Bio-veins and Ag@AgCl/Bio-veins(CI4) composite are depicted in Fig. 4. For the Bio-veins (Fig 4(a)), the peaks at 3331 and 1593 cm^{-1} of the samples are closely linked to stretching vibration of internal H_2O molecules and surface O–H groups. The absorption peak located at 2913 cm^{-1} is attributed to the C–H stretching vibrations [31], and the absorption band around 1419 cm^{-1} corresponded to the CH_2 bending vibrations [32]. The absorption peaks positioned at 1263, 1222, and 1024 cm^{-1} are derived from the –COO vibrations and C–O–C [33]. Compared to the blank Bio-veins, the Ag@AgCl/Bio-veins(CI4) composite shows almost the same infrared spectrum, demonstrating that neither the impregnation-precipitation process nor the photoreduction process would change the structure of the Bio-veins. Besides, no AgCl absorption bands are observed, possibly resulting from the low content and homogeneous distribution of AgCl on the Bio-veins.

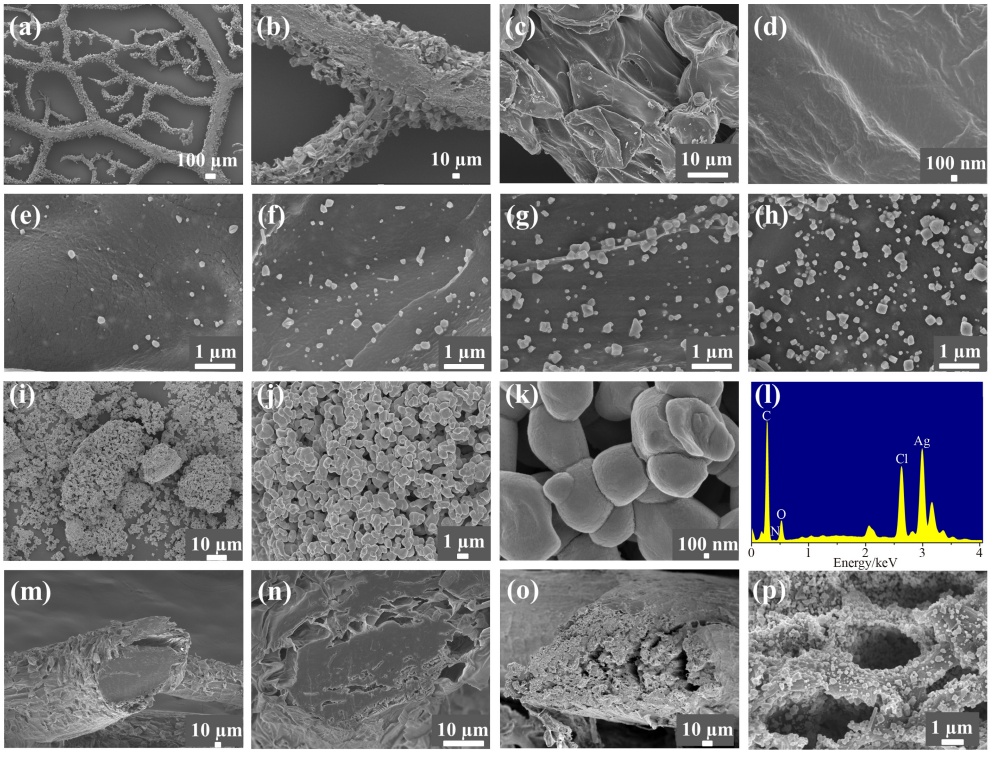

Fig. 3 The surface SEM images of (a–d) blank Bio-veins, (e–h) Ag@AgCl/Bio-veins(CI1, CI2, CI3, and CI4) composites, (i–k) pure Ag@AgCl, (l) EDS plane scan spectrum of CI4, the cross-sectional SEM images of (m, n) blank Bio-veins, and (o, p) Ag@AgCl/Bio-veins(CI4).

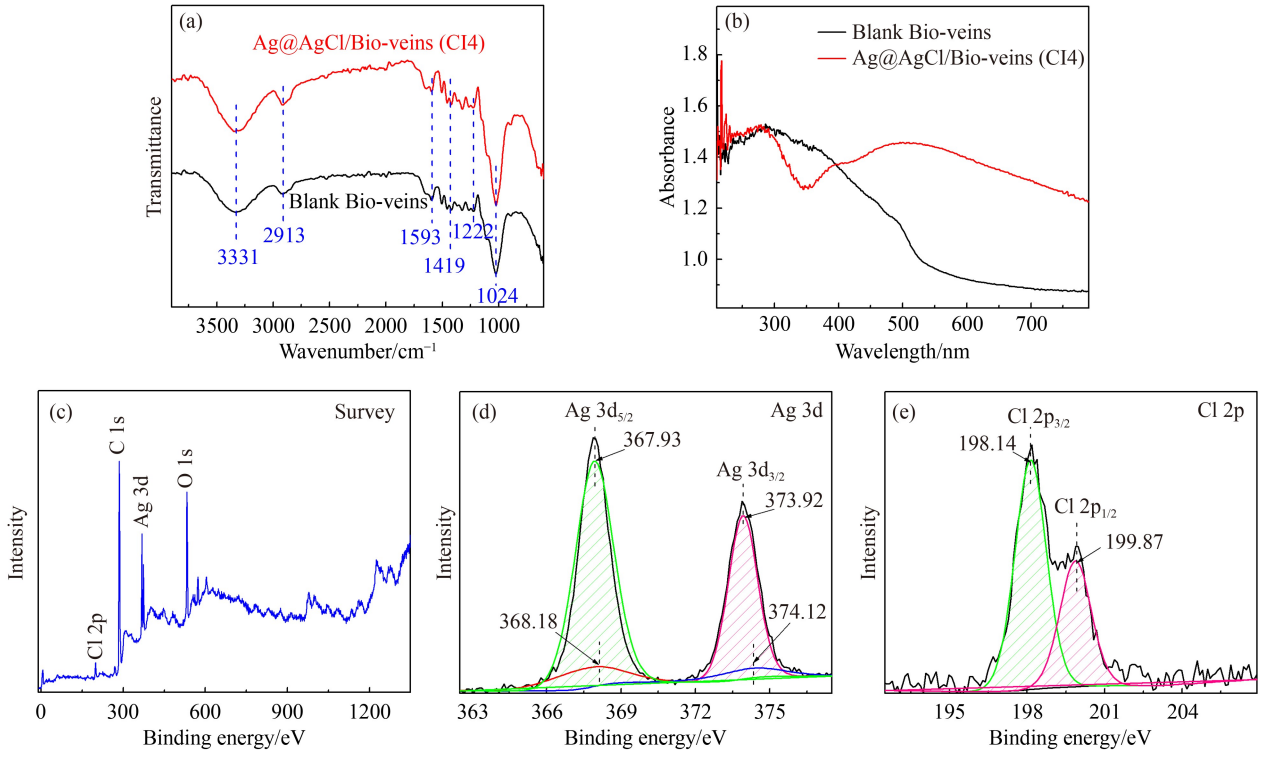

Fig. 4 (a) FTIR spectra and (b) DRS spectra of blank Bio-veins and Ag@AgCl/Bio-veins(CI4). XPS spectra of (c) survey scan, (d) Ag 3d and (e) Cl 2p of Ag@AgCl/Bio-veins(CI4).

The UV-vis DRS of the blank Bio-veins and Ag@AgCl/Bio-veins(CI4) composite are presented in Fig. 4(b). For the blank Bio-veins, we observe a high sensitivity in the ultraviolet light region, with a relatively weak absorption within the visible light range. That is largely due to the special biomass components (cellulose, lignin, and hemicellulose) which could efficiently adsorb UV light. For the Ag@AgCl/Bio-veins(CI4) composite, a new broad adsorption peak (450 to 650 nm) appears and the intensity of the visible light absorption peak increases significantly. This phenomenon can be ascribed to the LSPR effect of Ag, which is consistent with the results of previous similar studies [34].

The XPS spectra were performed to clarify the composition and valence state of the surface element in the Ag@AgCl/Bio-veins(CI4). As shown in Fig. 4(c), Ag, Cl, C, and O elements appear in the full scan spectrum of the tested sample. In Fig. 4(d), two peaks observed at 367.93 and 373.92 eV can be identified as Ag $3d_{5/2}$ and Ag $3d_{3/2}$, which are characteristic of Ag^+ in the AgCl particles, and the peaks at 368.18 and 374.12 eV are assigned to metallic Ag [35]. The spectrum of Cl 2p is given in Fig. 4(e), two peaks at 198.14 and 199.87 eV are clearly identified from the Cl 2p core level spectra, confirming the presence of Cl^- in AgCl [36]. The XPS results are in good agreement with the XRD results, further proving the co-existence of Ag with AgCl in the Ag@AgCl/Bio-veins.

3.2 Photocatalytic performance research under visible light

As a common synthetic dye, RhB was employed to evaluate the photocatalytic performance of the different materials under visible irradiation, and the obtained data are presented in Fig. 5. As reported in Fig. 5(a), in the blank control experiment, the concentration of RhB barely decreases without adding any photocatalyst, indicating that the self-degradation of RhB could be ignored and it would not affect the photocatalytic experiment. After adding the Ag@AgCl/Bio-veins(CI*x*) composite photocatalysts, the concentration of the RhB solution decreases significantly. Furthermore, as the value of soaking time (*x*) increases from 1 to 4, the degradation efficiency of the composites greatly increases from 78.9% to 99.7%. This may be down to the growing number of Ag@AgCl NPs on the Bio-veins with increased soaking time, which is consistent with the SEM results. Thus, the Ag@AgCl/Bio-veins(CI4) composite is considered to be the most appropriate photocatalyst in this work. To determine the different roles of Ag@AgCl and Bio-veins in the composite materials, the photocatalytic activities of pure Ag@AgCl, blank Bio-veins, and Ag@AgCl/Bio-veins(CI4) are compared in detail (Fig. 5(b)). For the blank Bio-veins, 26% of RhB is removed in 30 min in the dark experiment, confirming the good adsorption performance toward RhB. For pure Ag@AgCl (6.0 mg, which is the same weight of Ag@AgCl loaded on the Ag@AgCl/Bio-veins(CI4) composite), RhB is degraded,

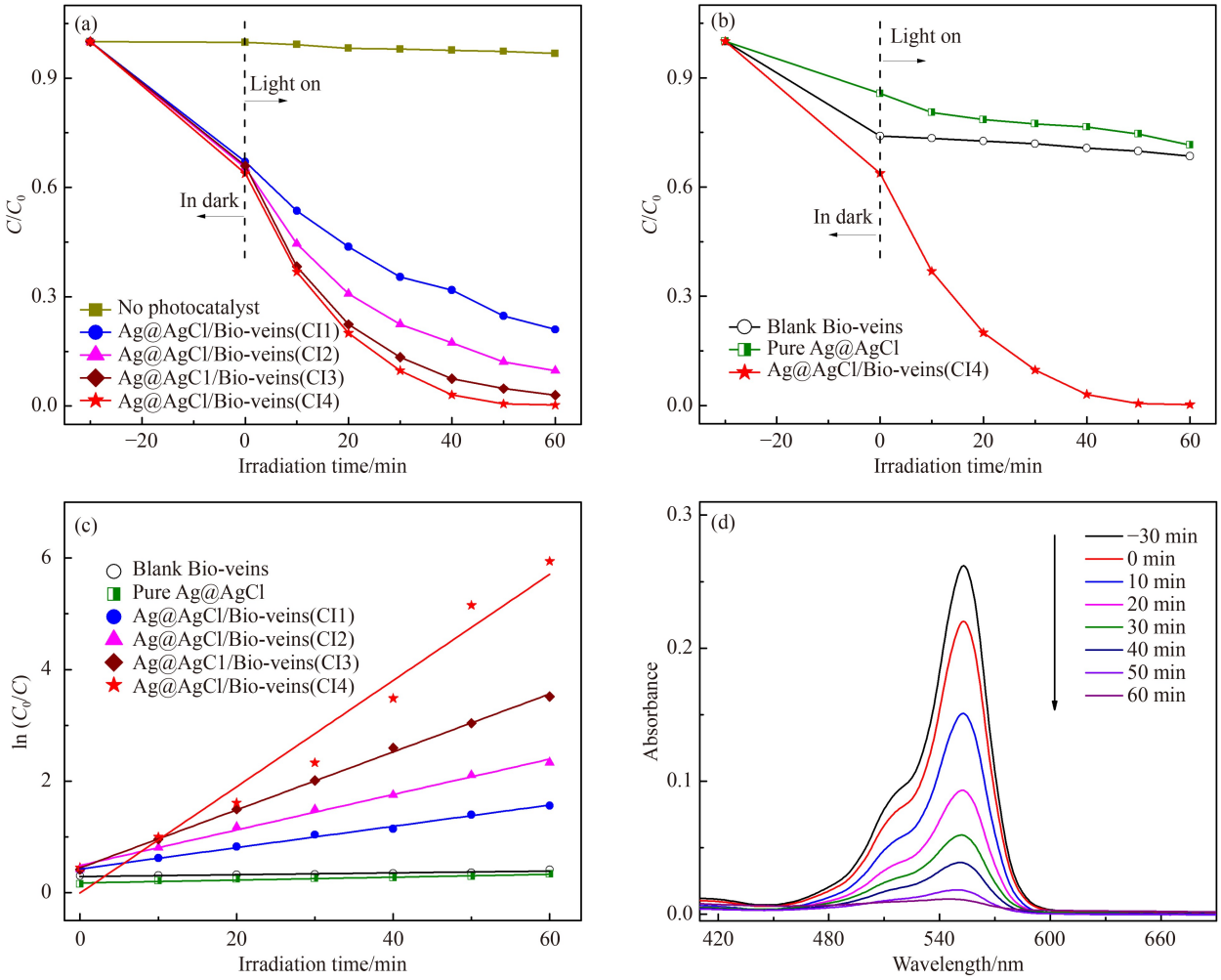

Fig. 5 (a) Degradation of RhB using Ag@AgCl/Bio-veins(CI*x*) composites; (b) curves of RhB relative to the concentration with the addition of blank Bio-veins, Ag@AgCl and Ag@AgCl/Bio-veins(CI4); (c) kinetic curves for RhB photodegradation by different samples; (d) optical absorption of the RhB solutions during the degradation process.

but the degradation efficiency is only 28.47%. By contrast, the Ag@AgCl/Bio-veins(CI4) composite displays considerably higher visible photocatalytic activity, the RhB removal efficiency is as high as 99.7%. The excellent photocatalytic activity of the Ag@AgCl/Bio-veins(CI4) composite could be explained in two aspects: (1) the good adsorption properties of the Bio-veins, and (2) the improved photocatalytic activity of the Ag@AgCl NPs loaded on the Bio-veins.

The photodegradation processes of RhB could be evaluated by the pseudo-first-order kinetic model [37]:

$$\ln(C_0/C) = kt, \quad (1)$$

where C_0 and C denote the concentration of RhB in the solution before and after reacting for t min, and k (min^{-1}) is the degradation rate constant. From Fig. 5(c), we find that all of the kinetic linear fitting curves of RhB degradation fit well with a linear behavior, which means that the photo-degradation processes of RhB by all materials could be explained by the pseudo-first-order kinetic model. The degradation rate constant (k) values were obtained from the slopes of the above lines. We find that the Ag@AgCl/Bio-veins(CI4) exhibits the maximum photodegradation rate of 95.1×10^{-3} min^{-1} among all samples, which is 59.44 times and 36.58 times higher than the blank Bio-veins (1.6×10^{-3} min^{-1}) and pure Ag@AgCl (2.6×10^{-3} min^{-1}), respectively. In contrast to other AgCl-based catalysts (Table 1), the Ag@AgCl/Bio-veins(CI4) in this study also demonstrates its outstanding photocatalytic performance.

Furthermore, the real-time changes of the RhB solution absorbance after adding the Ag@AgCl/Bio-veins(CI4) composite were also studied. The results are shown in Fig. 5(d), where the characteristic peak located at λ = 553 nm is assigned to RhB. The peak intensity decreases gradually with increasing visible light irradiation time and nearly disappears after 60 min. Furthermore, no other adsorption peaks appear within 200 to 800 nm, which signifies that RhB in the solution is completely degraded.

The stability and the reuse of a photocatalyst can be regarded as the critical factors in large-scale applications. The durability of the Ag@AgCl/Bio-veins(CI4) was

tested through repeat cycle experiments, and the results are exhibited in Fig. 6. The photoactivity of the Ag@AgCl/Bio-veins(CI4) decreased slightly after five successive cycles (Fig. 6(a)). The slight decrease may be down to two aspects, namely, (1) the inevitable loss of Ag@AgCl particles from the Bio-veins in the reaction and recovery processes, (2) gradual photocorrosion of the AgCl, where a large number of Ag^0 species formed on AgCl during the degradation process. The XRD pattern of the Ag@AgCl/Bio-veins(CI4) composite after the reaction could well prove the change in the phase structure of the photocatalyst. As shown in Fig. 6(b), new obvious characteristic peaks at 38.6°, 44.8°, and 64.9° appear, which are ascribed to Ag (JCPDS No. 04-0784). In addition, no Ag@AgCl powder was found to fall from the Bio-veins during the reaction or recycling processes. Thus, we can confirm that the Ag@AgCl NPs combine steadily with the Bio-veins.

3.3 Photocatalytic performance research under sunlight

An outdoor photocatalytic experiment under solar light irradiation was conducted to assess the practical application value of the composite. The optimal composite (Ag@AgCl/Bio-veins(CI4)) was used as the photocatalyst in this experiment. The same leaf-shaped composite was re-used for three consecutive days, the corresponding experimental results are recorded in Fig. 7. As we expected, the self-degradation of RhB under sunlight within 5 h was rather low. The RhB self-degradation rate values are all lower than 3% for the three consecutive days, which is negligible. It is satisfying that the Ag@AgCl/Bio-veins(CI4) composite also exhibits high photocatalytic efficiency and stability under sunlight, which is beneficial for practical applications. In addition, compared to the powdery Ag@AgCl, the recycling process of the Ag@AgCl/Bio-veins after the reaction is much easier, energy-saving and time-saving. Based on the aforementioned advantages, the Ag@AgCl/Bio-veins shows decent potential in the field of wastewater treatment.

3.4 Photodegradation mechanism

Radical capture experiments were conducted to determine the reactive radicals which greatly contribute to the photodegradation of RhB. In particular, 10 $mmol \cdot L^{-1}$ of IPA, TEOA and TEMPO were used as scavengers for the ·OH, $\cdot O_2^-$, and h^+ radicals, respectively [43]. As reported in Fig. 8, the efficiency of RhB degradation is almost invariable after adding IPA. By contrast, the addition of TEMPO and TEOA has a great influence on the photo-degradation process, and the degradation efficiency drops from 99.7% to 51.24% and 18.44% after adding TEMPO and TEOA, respectively (Fig. 8(b)). These experimental data manifest that $\cdot O_2^-$ and h^+ are the primary active

Table 1 Performance of different Ag@AgCl-based composites for the photodegradation of RhB under visible light

Photocatalyst	Photocatalyst form	Catalyst dosage/($g \cdot L^{-1}$)	RhB concentration/($mg \cdot L^{-1}$)	Degradation/%	Time/min	Ref.
AgCl/TiO_2/fly-ash	Granule	1	12.5	180	94.96	[38]
(Ag@AgCl)-Fe_3O_4/RGO	Powder	2	10	120	97.9	[39]
Ag@AgCl-TiO_2/FAC	Powder	–	2	120	96.68	[40]
Ag@AgCl-PU/SF	Slice	1	10	120	97	[7]
Ag/AgCl@ZIF-8	Powder	0.5	10	90	99.12	[41]
Ag/AgCl/NC	Powder	0.4	10	60	>95	[42]
Ag@AgCl/Bio-veins(CI4)	Slice	0.7	10	60	99. 7	This work

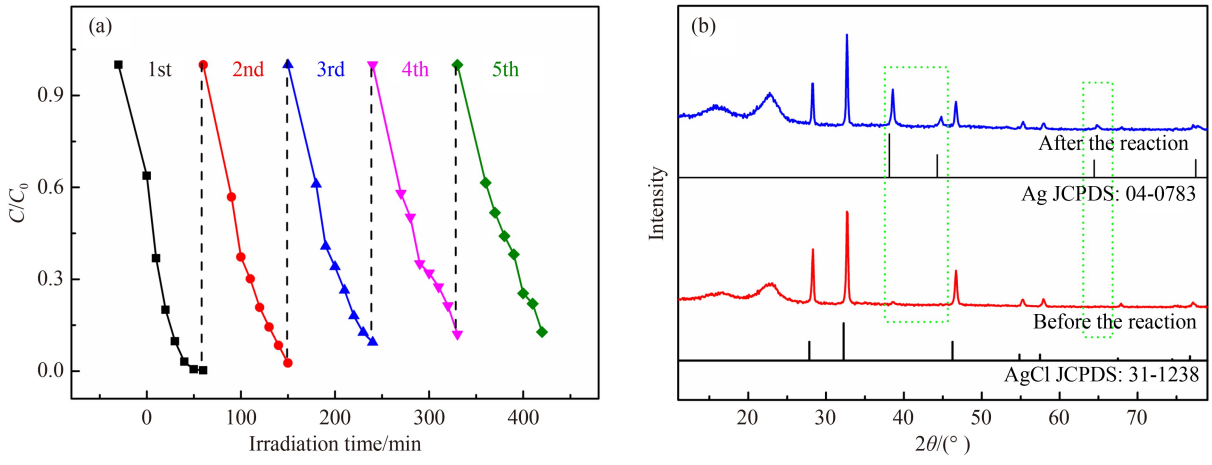

Fig. 6 (a) Cycling experiments of the Ag@AgCl/Bio-veins(CI4); (b) XRD patterns of the Ag@AgCl/Bio-veins(CI4) before and after the cycling experiments.

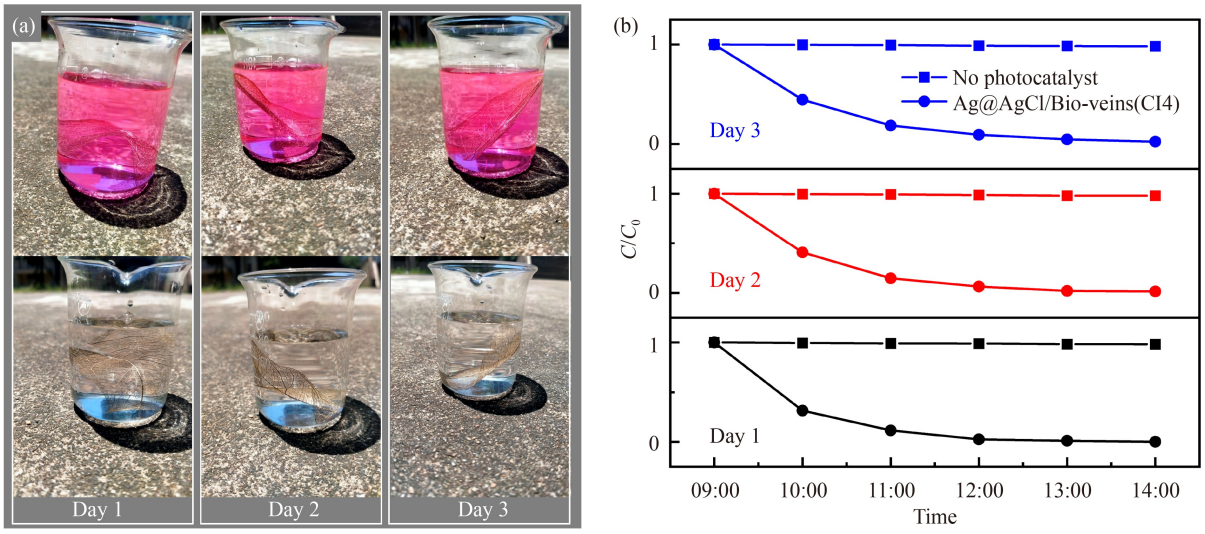

Fig. 7 (a) Photos of the reaction system before and after degradation under sunlight; (b) photocatalytic degradation curves of Ag@AgCl/Bio-veins(CI4) for RhB in three consecutive days.

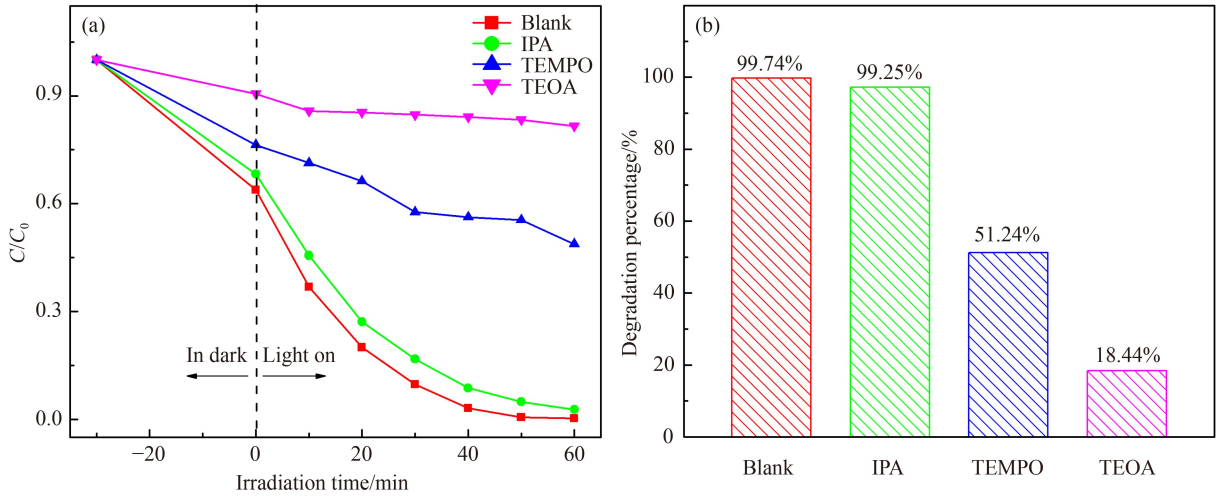

Fig. 8 (a) Curves of RhB relative concentration with the addition of different scavengers; (b) the degradation percentage of RhB by the Ag@AgCl/Bio-veins(CI4) composite after the introduction of different scavengers.

species in the photodegradation process of RhB.

As indicated in previous studies [44,45], AgCl can be considered a wide bandgap semiconductor (about 3.25 eV) and difficult to be excited by visible light, thus, single AgCl materials will not be suitable as photocatalysts. However, after the photoreduction process under UV light irradiation, some of the Ag^+ ions are reduced to Ag^0 in the AgCl material. The surface polarization behavior of the AgCl NPs could be terminated by Cl^-, leading to the negatively charged AgCl NPs. Attributing to the LSPR effect of the Ag NPs, the Ag@AgCl particles possess a strong visible light response and could be considered an efficient photocatalyst. According to the experimental results and analysis, a plausible photocatalytic mechanism for RhB by using Ag@AgCl/Bio-veins was proposed. As depicted in Fig. 9, first, the visible or solar light is absorbed by the Ag NPs and e^-/h^+ pairs are produced on the Ag surface. Because of the strong LSPR effect of Ag NPs and the polarization of the AgCl NPs, photogenerated electrons are transferred from Ag NPs to the conduction band (CB) of AgCl NPs. Then, the e^- in the CB of AgCl could capture O_2 molecules to create superoxide radical ($\cdot O_2^-$), and positively charged holes transfer from Ag to the AgCl NPs, and Cl^- ions are oxidized to Cl^0 atoms. Both the $\cdot O_2^-$ and Cl^0 atoms would further participate in the degradation process of the RhB molecules, and the RhB molecules are decomposed into inorganic small molecules such as CO_2 and H_2O. The reaction processes are written as Eqs. (2)–(8).

$$Ag^0(LSPR) \xrightarrow{h\nu} Ag(e^-) + Ag(h^+) \quad (2)$$

$$Ag(e^-) + AgCl \rightarrow Ag + AgCl(e^-) \quad (3)$$

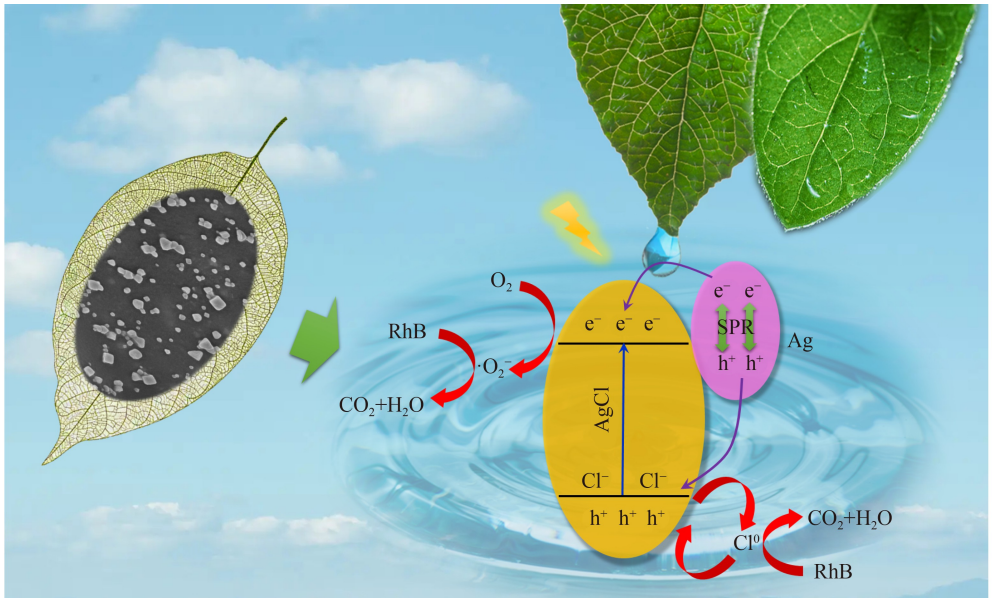

Fig. 9 Schematic illustration of the Ag@AgCl/Bio-veins photocatalytic mechanism.

$$AgCl(e^-) + O_2 \rightarrow AgCl + \cdot O_2^- \quad (4)$$

$$Ag(h^+) + AgCl \rightarrow Ag + AgCl(h^+) \quad (5)$$

$$AgCl(h^+) + Cl^- \rightarrow AgCl + Cl^0 \quad (6)$$

$$\cdot O_2^- + RhB \rightarrow CO_2 + H_2O \quad (7)$$

$$Cl^0 + RhB \rightarrow CO_2 + H_2O \quad (8)$$

In addition, the Bio-veins also plays a vital part in the photocatalytic process of RhB. First, the Bio-veins as a carrier could effectively immobilize the Ag@AgCl NPs, preventing their aggregation. Second, the existence of Bio-veins could also affect the crystal appearance and crystallite size of the Ag@AgCl NPs. Third, the special microporous surface topography and abundant functional groups of the Bio-veins (hydroxyl, carbonyl, and aromatic rings) [46,47] not only promote RhB adsorption, but also provide more active sites for photocatalytic degradation. All of these are useful for the improvement of photocatalytic activity.

4 Conclusions

A novel Ag@AgCl/Bio-veins composite photocatalyst was synthesized using a facile impregnation-precipitation-photoreduction method. The Ag@AgCl NPs were uniformly and firmly anchored to the Bio-veins matrix. Compared to the pure Ag@AgCl NPs and Bio-veins, the Ag@AgCl/Bio-veins composite materials showed significantly higher photocatalytic activity for the degradation of RhB. Active radical experiments revealed that both $\cdot O_2^-$ and h^+ were the major active species for the photodegradation of RhB, and a plausible photocatalytic mechanism was proposed. Moreover, with a macroscopic fiber substrate, the recycling process of the Ag@AgCl/Bio-veins after reaction was much easier to implement and showed better energy savings. After removal from the solution by tweezers, the Ag@AgCl/Bio-veins was reused five times with no obvious loss in photodegradation activity, indicating the excellent stability and reusability of the Ag@AgCl/Bio-veins. In summary, as a type of promising candidate for easy-to-recover photocatalyst, it was worth of research, and this synthesis procedure provided a new idea and approach for the preparation of nano-photocatalysts supported on biomass templates.

Acknowledgements This work was supported by the National Natural Science Foundation of China (Grant No. 21776067), the Outstanding Youth Foundation of Hunan Province (Grant No. 2020JJ2014), the Natural Science Foundation of Hunan Province (Grant Nos. 2022JJ30264, 2020JJ5159), and the Scientific Research Fund of Hunan Provincial Education Department (Grant Nos. 20C0803, 21B0476).

References

1. Wang Z B, Zhang L Y, Li N, Lei L, Shao M Y, Yang X, Song Y, Yu A M, Zhang H Q, Qiu F P. Ionic liquid-based matrix solid-phase dispersion coupled with homogeneous liquid–liquid microextraction of synthetic dyes in condiments. Journal of Chromatography A, 2014, 1348(27): 52–62
2. Alves S P, Brum D M, Branco de Andrade É C, Pereira Netto A D. Determination of synthetic dyes in selected foodstuffs by high performance liquid chromatography with UV-DAD detection. Food Chemistry, 2008, 107(1): 489–496
3. Sultan M. Polyurethane for removal of organic dyes from textile wastewater. Environmental Chemistry Letters, 2017, 15(2): 347–366
4. Tichapondwa S M, Newman J P, Kubheka O. Effect of TiO_2

phase on the photocatalytic degradation of methylene blue dye. Physics and Chemistry of the Earth Parts A/B/C, 2020, 118−119: 102900

5. Varjani S, Rakholiya P, Ng H Y, You S, Teixeira J A. Microbial degradation of dyes: an overview. Bioresource Technology, 2020, 314: 123728
6. Sutherland A J, Ruiz-Caldas M X, de Lannoy C F. Electro-catalytic microfiltration membranes electrochemically degrade azo dyes in solution. Journal of Membrane Science, 2020, 611: 118335
7. Zhou H, Wang X H, Wang T F, Zeng J X, Yuan Z Q, Jian J, Zhou Z H, Zeng L W, Yang H Z. *In situ* decoration of Ag@AgCl nanoparticles on polyurethane/silk fibroin composite porous films for photocatalytic and antibacterial applications. European Polymer Journal, 2019, 118: 153–162
8. Zhou H, Zhou J, Wang T F, Zeng J X, Liu L H, Jian J, Zhou Z H, Zeng L W, Liu Q Q, Liu G Q. *In-situ* preparation of silver salts/collagen fiber hybrid composites and their photocatalytic and antibacterial activities. Journal of Hazardous Materials, 2018, 359: 274–280
9. Han N, Yao Z X, Ye H, Zhang C, Liang P, Sun H Q, Wang S B, Liu S M. Efficient removal of organic pollutants by ceramic hollow fibre supported composite catalyst. Sustainable Materials and Technologies, 2019, 20: e00108
10. Wang S, Zhang W, Jia F C, Fu H L, Liu T T, Zhang X, Liu B, Núñez-Delgado A, Han N. Novel Ag_3PO_4/boron-carbon-nitrogen photocatalyst for highly efficient degradation of organic pollutants under visible-light irradiation. Journal of Environmental Management, 2021, 292: 112763
11. Gou J F, Li X H, Zhang H X, Guo R N, Deng X Y, Cheng X W, Xie M Z, Cheng Q F. Synthesis of silver/silver chloride/exfoliated graphite nano-photocatalyst and its enhanced visible light photocatalytic mechanism for degradation of organic pollutants. Journal of Industrial and Engineering Chemistry, 2018, 59: 99–107
12. Guo C F, Sun T Y, Wang Y, Gao J W, Liu Q, Kempa K, Ren Z F. Conductive black silicon surface made by silver nanonetwork assisted etching. Small, 2013, 9(14): 2415–2419
13. Choi M, Shin K, Jang J. Plasmonic photocatalytic system using silver chloride/silver nanostructures under visible light. Journal of Colloid and Interface Science, 2010, 341(1): 83–87
14. Zou Y J, Huang H, Li S S, Wang J, Zhang Y. Synthesis of supported Ag/AgCl composite materials and their photocatalytic activity. Journal of Photochemistry and Photobiology A: Chemistry, 2019, 376: 43–53
15. Zhou P F, Shen Y B, Zhao S K, Li G D, Cui B Y, Wei D Z, Shen Y S. Zhou P, Shen Y, Zhao S, Bai J, Han C, Liu W, Wei D. Facile synthesis of clinoptilolite-supported Ag/TiO_2 nanocomposites for visible-light degradation of xanthates. Journal of the Taiwan Institute of Chemical Engineers, 2021, 122: 231–240
16. Wang X H, Sui Y G, Jian J, Yuan Z Q, Zeng J X, Zhang L, Wang T F, Zhou H. Ag@AgCl nanoparticles *in-situ* deposited cellulose acetate/silk fibroin composite film for photocatalytic and antibacterial applications. Cellulose, 2020, 27(13): 7721–7737
17. Wang X H, Jian J, Yuan Z Q, Zeng J X, Zhang L, Wang T F, Zhou H. *In situ* loading of polyurethane/negative ion powder composite film with visible-light-responsive Ag_3PO_4@AgBr particles for photocatalytic and antibacterial applications. European Polymer Journal, 2020, 125: 109515
18. Wu M, Yan L T, Li J L, Wang L. Synthesis and photocatalytic performance of Ag/AgCl/ZnO tetrapod composites. Research on Chemical Intermediates, 2017, 43(11): 6407–6419
19. Sun L L, Yin S K, Shen D, Zhou Y J, Li J Z, Li X, Wang H Q, Huo P W, Yan Y S. Fabricating acid-sensitive controlled PAA@Ag/AgCl/CN photocatalyst with reversible photocatalytic activity transformation. Journal of Colloid and Interface Science, 2020, 580: 753–767
20. Zhu H G, Chen D Y, Li N J, Xu Q F, Li H, He J H, Lu J M. Cyclodextrin-functionalized Ag/AgCl foam with enhanced photocatalytic performance for water purification. Journal of Colloid and Interface Science, 2018, 531: 11–17
21. Yuan Z Q, Dai W, Zhang S H, Wang F X, Jian J, Zeng J X, Zhou H. Heterogeneous strategies for selective conversion of lignocellulosic polysaccharides. Cellulose, 2020, 29(6): 3059–3077
22. Gao N L, Lu Z Y, Zhao X X, Zhu Z, Wang Y S, Wang D D, Hua Z F, Li C X, Huo P W, Song M S. Enhanced photocatalytic activity of a double conductive $C/Fe_3O_4/Bi_2O_3$ composite photocatalyst based on biomass. Chemical Engineering Journal, 2016, 304: 351–361
23. Xu L N, Shu Z, Feng L L, Zhou J, Li T T, Zhao Z L, Wang W B. Fresh biomass derived biochar with high-load zero-valent iron prepared in one step for efficient arsenic removal. Journal of Cleaner Production, 2022, 352: 131616
24. Alsaiari M. Biomass-derived active carbon (AC) modified TiO_2 photocatalyst for efficient photocatalytic reduction of chromium(VI) under visible light. Arabian Journal of Chemistry, 2021, 14(8): 103258
25. Peñas-Garzón M, Abdelraheem W, Belver C, Rodriguez J, Bedia J, Dionysiou D. TiO_2-carbon microspheres as photocatalysts for effective remediation of pharmaceuticals under simulated solar light. Separation and Purification Technology, 2021, 275: 119169
26. Zhou H, Qu W J, Wu M, Yuan Z Q, Jian J, Zhang L, Huang T F. Synthesis of novel BiOBr/Bio-veins composite for photocatalytic degradation of pollutants under visible-light. Surfaces and Interfaces, 2022, 28: 101668
27. Periasamy V S, Athinarayanan J, Alshatwi A. Bio-inspired plant leaf skeleton based three dimensional scaffold for three dimensional cell culture. Sustainable Chemistry and Pharmacy, 2020, 18: 100321
28. Song X C, Wachemo A C, Zhang L, Bai T Q, Li X J, Zuo X Y, Yuan H R. Effect of hydrothermal pretreatment severity on the pretreatment characteristics and anaerobic digestion performance of corn stover. Bioresource Technology, 2019, 289: 121646
29. Patil M P, Piad L L A, Bayaraa E, Subedi P, Tarte N H, Kim G D. Doxycycline hyclate mediated silver-silver chloride nanoparticles and their antibacterial activity. Journal of Nanostructure in Chemistry, 2019, 9(1): 53–60
30. Kumar-Krishnan S, Prokhorov E, Hernández-Iturriaga M, Mota-Morales J, Vázquez-Lepe M, Kovalenko Y, Sanchez I, Luna-Bárcenas G. Chitosan/silver nanocomposites: synergistic

antibacterial action of silver nanoparticles and silver ions. European Polymer Journal, 2015, 67: 242–251

31. Kargarzadeh H, Ahmad I, Abdullah I, Dufresne A, Zainudin S Y, Sheltami R M. Effects of hydrolysis conditions on the morphology, crystallinity, and thermal stability of cellulose nanocrystals extracted from kenaf bast fibers. Cellulose, 2012, 19(3): 855–866
32. Stevulova N, Hospodarova V, Estokova A, Singovszka E, Holub M, Demcak S, Briancin J, Geffert A, Kacik F, Vaclavik V, Dvorsky T. Characterization of manmade and recycled cellulosic fibers for their application in building materials. Journal of Renewable Materials, 2019, 7(11): 1121–1145
33. Suciyati S W, Manurung P, Sembiring S, Situmeang R. Comparative study of Cladophora sp. cellulose by using FTIR and XRD. Journal of Physics: Conference Series, 2021, 1751(1): 012075
34. Yao X X, Liu X H, Zhu D, Zhao C B, Lu L D. Synthesis of cube-like Ag/AgCl plasmonic photocatalyst with enhanced visible light photocatalytic activity. Catalysis Communications, 2015, 59: 151–155
35. Wang S J, Luo T, Zhu J, Zhang X M, Su S P. A facile way to fabricate cellulose-Ag@AgCl composites with photocatalytic properties. Cellulose, 2016, 23(6): 3737–3745
36. Daupor H, Wongnawa S. Urchinlike Ag/AgCl photocatalyst: synthesis, characterization, and activity. Applied Catalysis A: General, 2014, 473: 59–69
37. Yang S F, Niu C G, Huang D W, Zhang H, Zeng G M. Ag/AgCl nanoparticles-modified $CdSnO_3{\cdot}3H_2O$ nanocubes photocatalyst for the degradation of methyl orange and antibiotics under visible light irradiation. Journal of Colloid and Interface Science, 2017, 505: 96–104
38. Huo P W, Yan Y S, Li S T, Li H M, Huang W H. Floating photocatalysts of fly-ash cenospheres supported $AgCl/TiO_2$ films with enhanced Rhodamine B photodecomposition activity. Desalination, 2010, 256(1−3): 196–200
39. Zhong S T, Jiang W, Han M, Liu G Z, Zhang N, Lu Y. Graphene supported silver@silver chloride & ferroferric oxide hybrid, a magnetically separable photocatalyst with high performance undervisible light irradiation. Applied Surface Science, 2015, 347: 242–249
40. Liu S M, Zhu J L, Yang Q, Xu P P, Ge J H, Guo X T. Synthesis and characterization of cube-like Ag@AgCl-doped TiO_2/fly ash cenospheres with enhanced visible-light photocatalytic activity. Optical Materials, 2016, 53: 73–79
41. Zuo G H, Wang A Q, Yang Y, Huang H L, Wang F B, Jiang H W, Zhang L, Zheng Y J. Fabrication and characterization of Ag/AgCl@ZIF-8 hybrid nanostructure and used it as photocatalyst for degradation of Rhodamine B under visible light. Journal of Porous Materials, 2020, 27(2): 339–345
42. Wu Y H, Chen S S, Guo X H, Wu J N, Peng B H, Liu Z Y. Environmentally benign chitosan as precursor and reductant for synthesis of Ag/AgCl/N-doped carbon composite photocatalysts and their photocatalytic degradation performance. Research on Chemical Intermediates, 2017, 43(7): 3677–3690
43. Shi H F, Yan G, Zhang Y, Tan H Q, Zhou W Z, Ma Y Y, Li Y G, Chen C L, Wang E B. $Ag/Ag_xH_{3-x}PMo_{12}O_{40}$ nanowires with enhanced visible-light-driven photocatalytic performance. ACS Applied Materials & Interfaces, 2017, 9(1): 422–430
44. Xu D B, Shi W D, Song C J, Chen M, Yang S B, Fan W Q, Chen B Y. In-situ synthesis and enhanced photocatalytic activity of visible-light-driven plasmonic $Ag/AgCl/NaTaO_3$ nanocubes photocatalysts. Applied Catalysis B: Environmental, 2016, 191: 228–234
45. Tang Y Y, Wang W T, Wang B Z, Sun X, Guo C Y, Xu J. A novel AgCl-based visible-light photocatalyst through *in-situ* assembly of carbon dots for efficient dye degradation and hydrogen evolution. Sustainable Materials and Technologies, 2021, 27: e00242
46. Kim Y, Park J, Bang J, Kim J, Kim J H, Hwang S W, Yeo H, Choi I G, Kwak H W. Highly persistent lignocellulosic fibers for effective cationic dye pollutant removal. ACS Applied Polymer Materials, 2022, 4(8): 6006–6020
47. Roa K, Oyarce E, Boulett A, ALSamman M, Oyarzún D, Pizarro G D C, Sánchez J. Lignocellulose-based materials and their application in the removal of dyes from water: A review. Sustainable Materials and Technologies, 2021, 29: e00320